Hindawi
Advances in Civil Engineering
Volume 2020, Article ID 7034517, 17 pages
https://doi.org/10.1155/2020/7034517

Research Article

A Study of Influence Distance and Road Safety Avoidance Distance from Postearthquake Building Debris Accumulation

Wei Wang,[1,2] **Nana Zhang**,[1] **Leiming Wang**,[1] **Ziyi Wang**,[1] **and Donghui Ma**[1,2]

[1]*Institute of Earthquake Resistance and Disaster Reduction, Beijing University of Technology, Beijing 100124, China*
[2]*College of Architecture and Urban Planning, Beijing University of Technology, Beijing 100124, China*

Correspondence should be addressed to Wei Wang; ieeww@bjut.edu.cn

Received 18 October 2019; Revised 15 January 2020; Accepted 29 January 2020; Published 21 February 2020

Academic Editor: Hayri Baytan Ozmen

To study the influence of the debris accumulation caused by the continuous collapse of the postearthquake building structure on the avoidance distance of the road red line, taking the typical masonry structures of three stories, five stories, and seven stories as examples, this study simulates the process of sloughing collapse and the positive and negative collapse along the Z axis of the building structure under 28 different seismic conditions in details. Taking "the flying stones" into consideration, this study divides the influence distance of the collapsed building structure under earthquakes into (a) the safety distance during earthquakes and (b) the main influence distance of the debris accumulation after the earthquake. In this study, two types of movement laws of flying stones are analyzed statistically first. Then, the statistical analysis and hypothesis testing are carried out on the main influence distance of all the debris accumulation using the influence width coefficient, and the main influence distance distribution probability models of the debris accumulation of the collapsed building structure under earthquake excitation are established. The distribution models include the gamma distribution and the extreme value type III along the Z axis and the normal distribution probability model along the X axis. Finally, a simplified calculation table of the influence distance of collapsed building structures is established. It provides a scientific basis for the safe control distance of buildings to avoid the road red line and for the minimum distance between the buildings and people after a destructive earthquake.

1. Introduction

The collapse of buildings along the street not only poses a serious threat to people's lives and properties but also is the main influencing factor of postearthquake traffic capacity [1]. According to the statistics [2], there are 5.36 million buildings collapsed during the 2008 Wenchuan earthquake. The building collapse narrows the effective width of the road and seriously affects the road traffic capacity. In addition, it increases difficulties for the transportation of supplement, and the rescue and evacuation of the refugees after the earthquake. Figure 1 shows the ruins of buildings in Hanwang county blocked streets during the Wenchuan earthquake [3]. Thus, it is important to study the influence distance of the debris accumulation after building structures collapsed under earthquake excitation, and it is of great significance for postearthquake rescue and the formulation of urban planning.

Previous researchers estimated postearthquake debris obstruction of collapsed buildings and predicted the distribution of debris accumulation based on survey data of earthquake damage [4]. For example, Meguro and Hakuno [5] analyzed the main collapse modes of buildings along the street by using survey data and existing research results, and predict the debris area. Based on earthquake intensity and spatial characteristics, they further developed the seismic damage assessment model of buildings. Meanwhile, they also investigated the influence of building collapse on the road obstruction under the set ground motion intensity. Song and Li [6] proposed a calculation formula for debris obstruction based on the postearthquake debris distribution model [7] and developed a prediction model for debris obstruction of collapsed buildings. Argyroudis [8] proposed a brief geometric model of the building height and the distribution width of debris accumulation. It was assumed

Figure 1: The collapse of buildings blocking streets.

that the width of debris accumulation is consistent with the Gaussian distribution; that is, the exceeding probability of given width can be calculated when the building height is known. According to the seismic data of the Greek city of Thessaloniki, Argyroudis et al. [9] found that the most influential collapses on road obstruction were toppling, collapse of debris accumulation, and collapse of the extension layer. Furthermore, the distribution width of debris accumulation was calculated in their studies. Earthquake damage investigation is one of the most realistic and accurate methods. However, the seismic damage data are not comprehensive, and the occurrence of earthquake damage still has a great cost to the community.

Collapse mechanism and collapse modes of buildings have been used as the basis to study the distribution of debris accumulation and the influence distance of the collapsed building structure after the earthquake. With the continuous development of experimental methods and finite element theory, many researchers studied building collapse mechanism [10–12], collapse mode [13–15], and collapse resistant capacity [16]. The reasons for the collapse of the same structural form are different. For example, there are many different reasons for the collapse of the frame structure, such as axial compression ratio [17] and soft-story mechanism [18, 19]. Different reasons of collapse may cause different collapse modes; however, there are mainly three collapse modes of different building structure under earthquake, including local collapse, global tilt, and global collapse [3] (see Figure 2). Global collapse has a greater impact than the other two collapse modes. Furthermore, continuous collapse is one of the most common forms of global collapse.

Only a few researchers used experimental methods to predict and analyze the distribution of debris accumulation. Among them, Huang [20] studied the response of a three-story and one-span reinforced concrete frame structure model under the earthquake by shaking table test and recorded the reaction time-history and collapse process of the reinforced concrete frame structure under earthquake excitation. He also recorded distribution of debris accumulation after the model structure collapsed. Nevertheless, the operability of tests is low, and it has a great cost. In addition, the scaled model test is also prone to distortion.

Huang et al. [21] used a high-rise building as an example to study falling process of debris falling off the building envelope under earthquake and its distribution characteristics by using elastic time-history analysis. Based on this study, the safe and evacuation distance was defined. Xie et al. [22] analyzed the displacement and acceleration time-history response of the frame structures with masonry filled wall in different stories, and they calculated the number, distribution, and influence scope of debris of building structures under earthquake excitation. Based on a simulation test, Ma et al. [23] used a high-rise concrete frame-core tube structure [24] as an example to develop a formula for calculating the influence scope of collapsed buildings in the vertical progressive collapse mode. Although results obtained by using the numerical simulation method are more consistent with the actual situation, few studies have been conducted on the influence distance of debris accumulation after building structures collapsed.

Therefore, this study uses the ANSYS/LS-DYNA based on the principle of the central difference method [25], and inputs different ground motion records to simulate the process of the integer collapse of the building structure under earthquake excitation and statistically analyze distribution scope so as to obtain the minimum distance between people and buildings, and the impact and avoidance distance of roads after the earthquake.

2. Model Building and Working Condition Design

It is noted that the height of the building structure is an important contributing factor in investigating the collapse of the building structure. Therefore, three kinds of typical masonry structures with different building heights were used as the calculation model. The story numbers of the structural models were three, five, and seven, respectively, and the height of each story was 3 m. The walls of the buildings were made of MU10 fired common bricks and M5 masonry mortar, and the wall thickness was 240 mm. Cast-in-place reinforced concrete constructional columns were set at the junction of the longitudinal and cross walls of the building, and each story was provided with a ring beam at the height of the top of the window. The layout and elevation of the building structure are shown in Figures 3 and 4, respectively.

Based on homogenization theory [26] and the integral modeling method, this study used the plastic kinematic material to simulate the reinforced concrete and masonry wall materials. Moreover, the ground model was established with the No. 20 rigid material. The masonry material used the simplified stress-strain curve proposed by Shi [27, 28], the concrete material used was the constitutive relation suggested by E. Hognestad, and the steel material used was based on the elastoplastic constitutive relation of the criteria [29]. The failure criterion of the material was determined by the ultimate strain, and the material properties are shown in Table 1.

The upper structure uses the 3D solid element SOLID164, and the elements use a single point integration algorithm [30, 31]. SHELL163 was selected to simulate the ground, and the Belytschko-Tsay single point integral shell element algorithm was used.

(a) (b) (c)

Figure 2: The three collapse modes of the building structure. (a) Local collapse, (b) global tilt, and (c) global collapse.

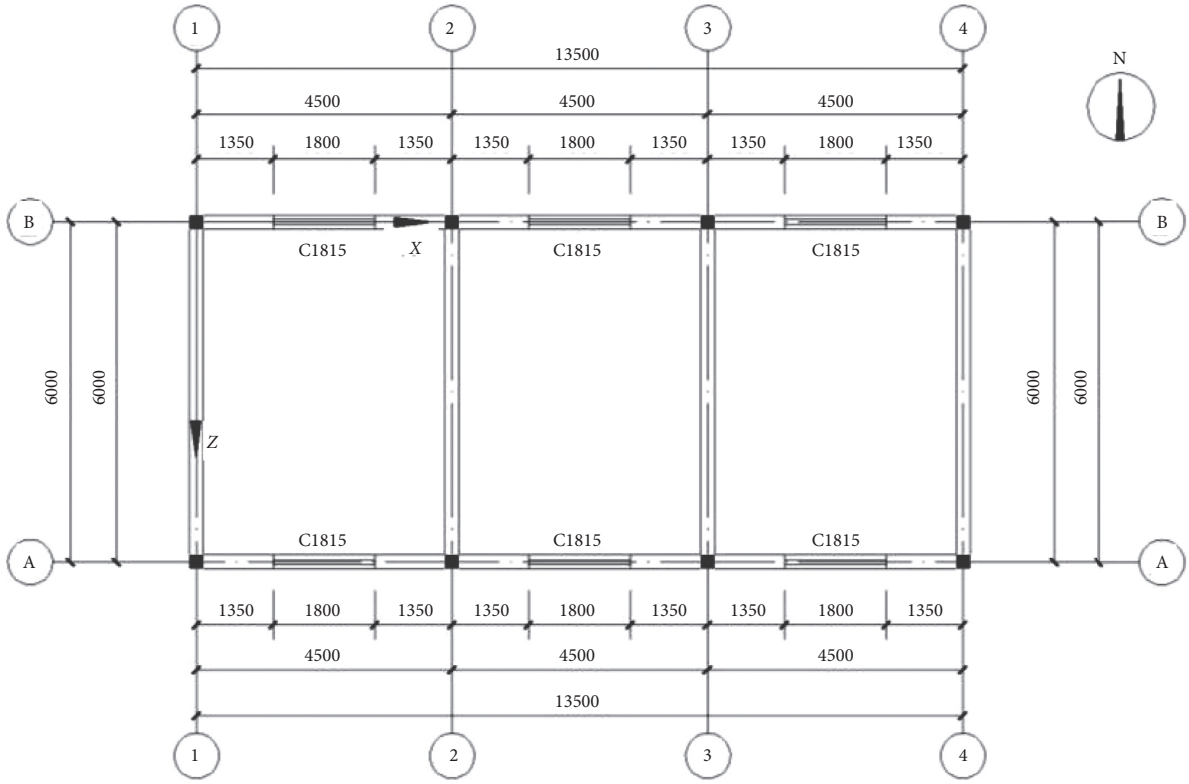

Figure 3: Layout of typical floor plan.

The element size of the masonry structure was taken as a regular hexahedron with a side length of 0.24 m, and the element size of the ground was taken as a regular quadrilateral with a side length of 20 m.

According to the empirical formula in the code [32], the basic period of a five-story masonry structure can be estimated to be 0.2722 s. The modal parameters such as periods and frequencies of the first three orders of the five-story masonry structure model were calculated by LS-DYNA calculation (see Table 2). The two calculation results are close, indicating that the calculated basic period has certain credibility.

Based on the random uncertainty of ground motion [33] and considering the theory of three essential elements of ground motion, seven ground motion records were chosen, namely, San Fernando wave, El Centro wave, Tianjin wave, El Centro #10 wave, Kobe wave, TCU068 Wave, and Wolongtai seismic wave. The peak of response spectrum of each seismic wave after amplitude modulation and its average were compared with the code response spectrum (see Figure 5). Four different peak accelerations were selected for each ground motion record. This simulation had a total of 28 working conditions (see Table 3) and 84 calculation processes. The direction of ground motion was applied along the direction of the structural cross wall, which was the positive direction of the Z axis.

3. Continuous Collapse Modes of Masonry Structure

The whole process of continuous collapse of each masonry structure under various working conditions is obtained through calculation. However, the seismic collapse process of building structures is very complicated and uncertain.

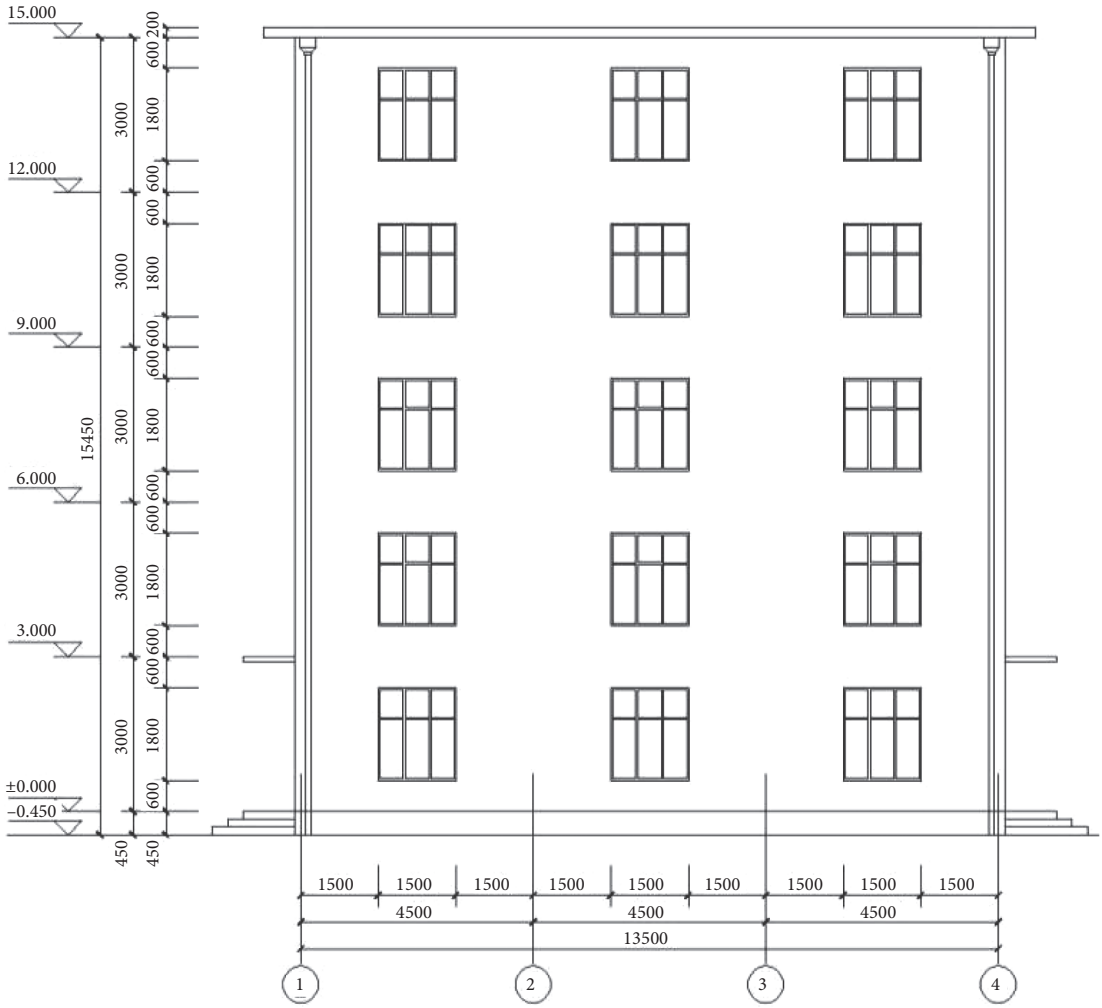

Figure 4: Elevation view of the building.

Table 1: Material properties.

Material	Density (kg/m³)	Elastic modulus (Pa)	Poisson's ratio	Yield stress (Pa)	Failure compressive strain	Failure tensile strain
Masonry wall	2200	2.25*e*9	0.15	2.83*e*6	0.0046	0.00056
Concrete	2700	2.73*e*10	0.2	1.72*e*7	0.0038	0.0007
Reinforcement	7800	2.0*e*5	0.3	3.35*e*8	—	0.01

Table 2: Periods and frequencies of the first three orders.

Order	1	2	3
Period (s)	0.2601	0.2425	0.1673
Frequency (Hz)	3.8443	4.1235	5.9785

Moreover, the collapse modes of building structures under different earthquakes are not identical. The collapse modes of the masonry structure under various working conditions can be divided into three kinds: sloughing collapse, and collapse in the positive and negative directions along the Z axis. The three-story masonry structure is more prone to sloughing collapse under various seismic conditions, and the five-story and seven-story masonry structures are more likely to collapse in the positive and negative directions along the Z-axis, but the degree of tilt is not exactly the same. To introduce the collapse process under various working conditions in detail, a five-story masonry structure is used as an example to illustrate the typical situation of each collapse mode:

The collapse process of the five-story masonry structure under the 26th working condition is shown in Figure 6. Cracks begin to occur at the junction between ground walls of the masonry structure and constructional columns at $t = 3.96$ s. As the damage continues, the ground walls are further damaged at $t = 4.86$ s, particularly the cross wall with

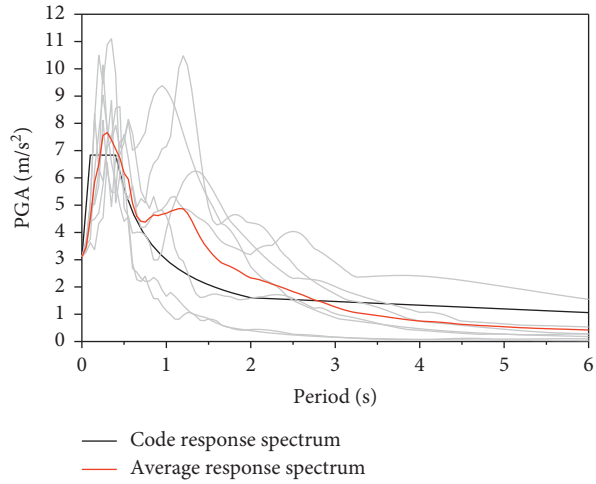

Figure 5: Comparison of seismic response spectrum mean and normative response spectrum.

Table 3: 28 working conditions.

PGA	Seismic wave						
	San Fernando	El Centro	Tianjin wave	El Centro #10	Kobe	TCU068	Wolongtai wave
0.8 g	1	5	9	13	17	21	25
1.0 g	2	6	10	14	18	22	26
1.2 g	3	7	11	15	19	23	27
1.5 g	4	8	12	16	20	24	28

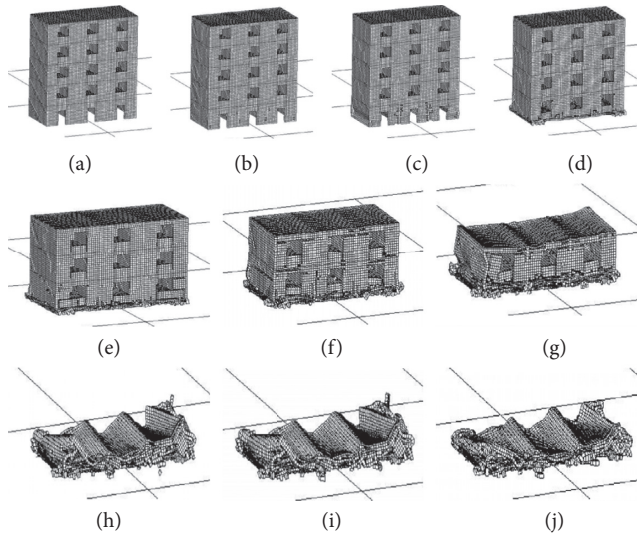

Figure 6: Collapse process of the five-story masonry structure under the 26th working condition. (a) $t = 0$ s, (b) $t = 3.96$ s, (c) $t = 4.86$ s, (d) $t = 5.66$ s, (e) $t = 6.09$ s, (f) $t = 6.48$ s (g) $t = 6.83$ s, (h) $t = 7.35$ s, (i) $t = 7.50$ s, and (j) $t = 10$ s.

bigger shear force and walls near the structural column, and at the corner of the doors and windows. With further damage, the whole structure begins to collapse downward. At $t = 5.66$ s, the upper plate of the ground floor hits the ground. While the structure continues to collapse and the cracks continue to develop, part walls of the structure are disintegrated. At $t = 6.09$ s, $t = 6.48$ s, $t = 6.83$ s, and $t = 7.35$ s, the upper plate of the structure layer collapses gradually from the second floor to the top floor. At $t = 7.5$ s, the structure is completely collapsed and destroyed, and the progressive collapse and destruction ends. The final debris accumulation is formed once time reached 10 s. The structural collapse mode is continuous sloughing collapse beginning with the collapse of the ground floor of the structure, followed by the structure collapsed downward from the ground floor to the top floor of the structure.

During the collapse process, a "flying rock" is shown in the constructional column (see Figure 7).

The collapse process of the five-story masonry structure under the 3rd working condition is shown in Figure 8. The collapse process of the structure under the 3rd working condition is similar to that under condition 26. The difference is that each key point of failure appears earlier. And the most important is that the structure tilts along the positive direction of the Z axis in the collapse process. The final debris accumulation is formed once time reached 10 s. The structural collapse mode under the 3rd working condition is continuous toppling collapse that begins with the collapse of the ground floor of the structure. Moreover, the structure collapses downward continuously from the ground floor to the top floor of the structure and topples along the positive direction of the Z axis.

The collapse process of the five-story masonry structure under the 14th working condition is shown in Figure 9. The collapse process of the structure under the 14th working condition is similar to that under condition 26. The difference is that each key point of failure appears earlier. And the most important is that the structure tilts along the negative direction of the Z axis in the collapse process. The final debris accumulation is formed once time reached 10 s. The structural collapse mode under the 14th working condition is continuous toppling collapse that begins with the collapse of the ground floor of the structure. The structure collapses downward continuously from the ground floor to the top floor of the structure and topples along the negative direction of the Z axis.

The directions of the collapse mainly depend on the damage degree of the bearing structures on the north and south sides of the masonry structure under earthquake excitation. When the masonry structure begins to topple and collapse, the damage degree of the bearing structure including walls and constructional columns on the south side is more severe than that on the north. With the forces from the gravity and seismic shear, the upper structure gradually topples and collapses along the positive direction of the Z axis. The collapse process of the whole structure appears as a positive toppling along the Z axis. On the contrary, when the damage degree of the bearing structure including walls and constructional columns on the north side is more severe than that on the south, the collapse process of the whole structure will appear as a negative toppling along the Z axis. When the damage degree of the bearing structure shows not much difference on either side, the structure will show sloughing collapse.

For a specific building structure, the collapse of the ground floor depends on the ground motion. In this case, the damage of the bearing structure of the ground floor affects the toppling direction of the upper structure under the earthquake.

4. Statistical Analysis of Influence Distance

The collapse of the structure under earthquake excitation is a high nonlinear problem of noncontinuum media and large deformation [34]. During the collapse process, the debris flies out because of friction, extrusion, and collision among the structural materials, and between the structure and the ground. These debris become flying stones. The calculation results show that the influence distance caused by the flying stone is generally larger than the main influence distance of debris accumulation. The influence distance of the collapsed building structure under earthquake excitation should be considered from two aspects. First, the main influence distance is the main distribution scope of debris accumulation outside the original building range after earthquake. The influence distance of the flying stone, which is far more than the main influence distance, is not considered. Second, the safety distance includes the main influence distance of the debris accumulation and the impact of the flying stone under earthquake excitation.

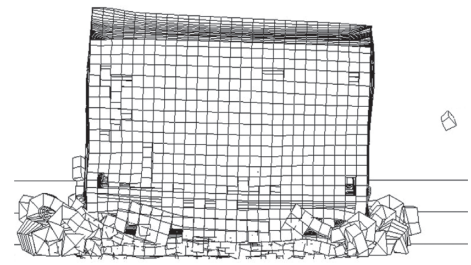

Figure 7: The flying stone element generated under the 26th working condition.

4.1. Statistical Analysis of the Main Influence Distance. Figure 10 shows the main influence scope of debris accumulation after the building structure collapses.

The input of seismic waves will cause the debris accumulation generated by the building collapse to be distributed around, so it is necessary to count the influence distance of the two directions, that is, the directions of the debris accumulation along the Z axis and the X axis. The input of seismic waves scatters the debris accumulation from the building. Thus, it is necessary to investigate the influence distance of both directions of the debris accumulation along the Z axis and the X axis.

4.1.1. Main Influence Distance along the Z Axis. The influence distance of unit height along the Z axis in the continuous collapse mode of the three-story, five-story, and seven-story masonry structures under various seismic conditions is statistically analyzed (see the influence width coefficient in Figure 11).

The discrete degrees of the above three figures are compared, and it is found that the influence width coefficient of the collapse of the three-layer masonry structure is clustered, showing that the three-story structure is more characterized by sloughing collapse under earthquake excitation. On the other hand, the influence coefficient of the seven-story masonry structure is relatively dispersed. This is because the seven-story masonry structure is more likely to topple under earthquake excitation, and its influence width has an obvious directionality.

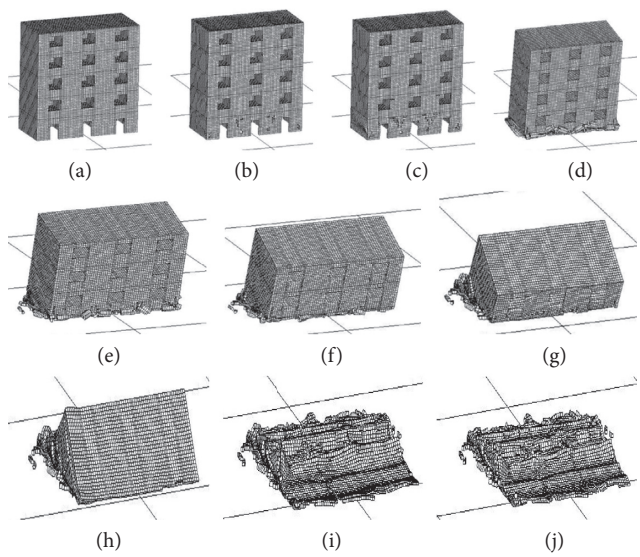

Figure 8: Collapse process of the five-story masonry structure under the 3rd working condition. (a) $t = 0$ s, (b) $t = 1.51$ s, (c) $t = 1.85$ s, (d) $t = 2.70$ s, (e) $t = 3.15$ s, (f) $t = 3.47$ s (g) $t = 3.80$ s, (h) $t = 4.02$ s, (i) $t = 4.85$ s, and (j) $t = 10$ s.

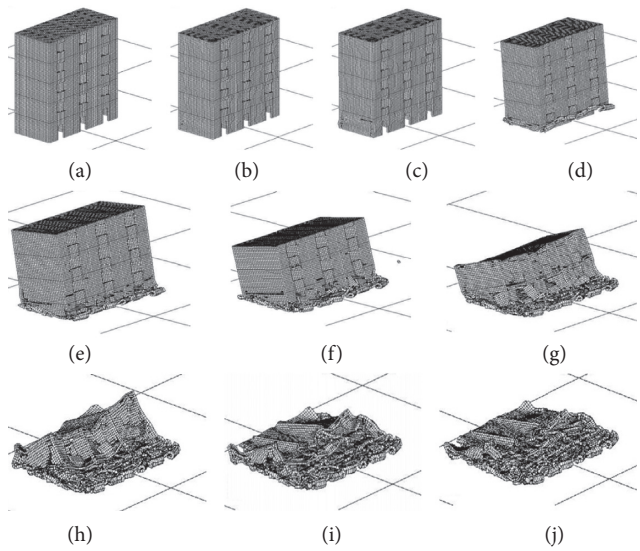

Figure 9: Collapse process of the five-story masonry structure under the 14th working condition. (a) $t = 0$ s, (b) $t = 1.35$ s, (c) $t = 2.00$ s, (d) $t = 2.74$ s, (e) $t = 3.16$ s, (f) $t = 3.56$ s (g) $t = 3.93$ s, (h) $t = 4.23$ s, (i) $t = 4.60$ s, and (j) $t = 10$ s.

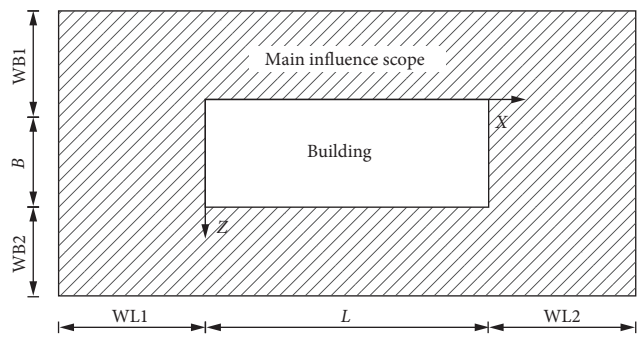

Figure 10: Main influence scope of debris accumulation of the collapsed building structure.

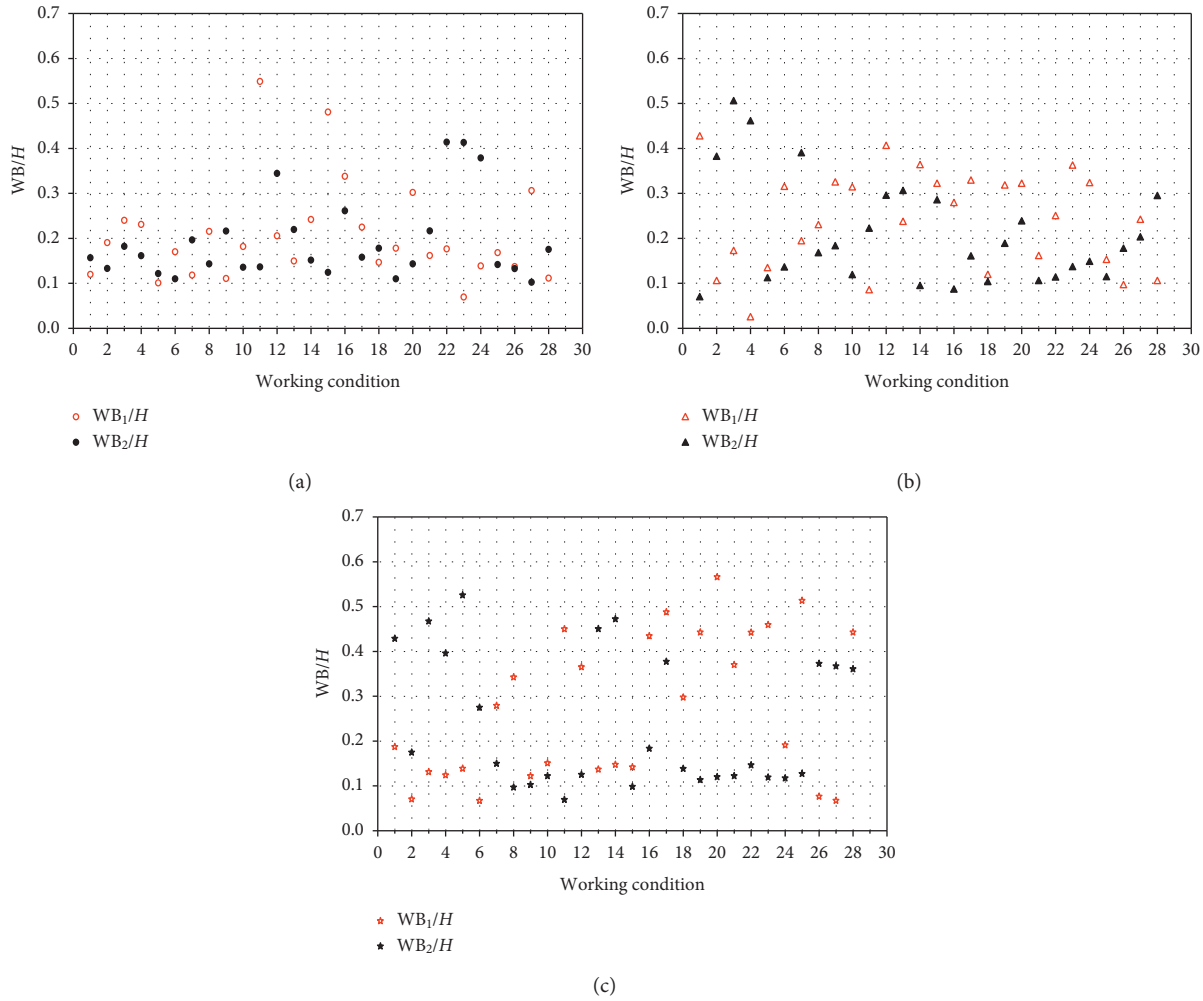

Figure 11: Width coefficient of influence along the Z axis of continuous collapse of masonry structure under various working conditions. (a) The three-story masonry structure along the Z axis, (b) the five-story masonry structure along the Z axis, and (c) the seven-story masonry structure along the Z axis.

According to the existing 84 calculation results, the maximum influence width coefficients WB_{max}/H are classified and statistically obtained. Figure 12 shows the frequency histogram.

4.1.2. Main Influence Distance along the X Axis. Similarly, the influence width coefficient of the structure along the X axis in the progressive collapse mode of the three-story, five-story, and seven-story masonry structures under various seismic conditions is statistically analyzed (see Figure 13).

The maximum influence width coefficient WL_{max}/H obtained from the calculation results is classified and statistically obtained, and the frequency histogram is shown in Figure 14.

The validity of numerical models is mostly obtained by comparison with experimental results [35, 36], but there are few experiments related to our research, so we compared the results of the study with previous theoretical calculations [37] we have done. The influence range of the debris accumulation after the building structure collapsed is calculated. And the coefficient change schematic diagram of structure directional collapse influence width is given (see Figure 15). According to Figure 15, the maximum influence width coefficient corresponding to the 3-story masonry structure in our simulation along the collapse direction is about 0.679.

By simulating the collapse of three-story masonry structure under 28 working conditions, the maximum influence width coefficient along the collapse direction is about 0.55 (see Figure 11(a)). Therefore, the result obtained through simulation is effective, and simulation is a feasible method to statistically analyze the influence distance of the debris accumulation of collapsed buildings after earthquake.

4.2. Statistical Analysis of Safety Distance. It is found that the occurrence of the "flying stones" is very common in the continuous collapse process. It is also found that the movement law of the "flying stones" can be divided into two cases. In the first case, the "flying stones" do not fail in the

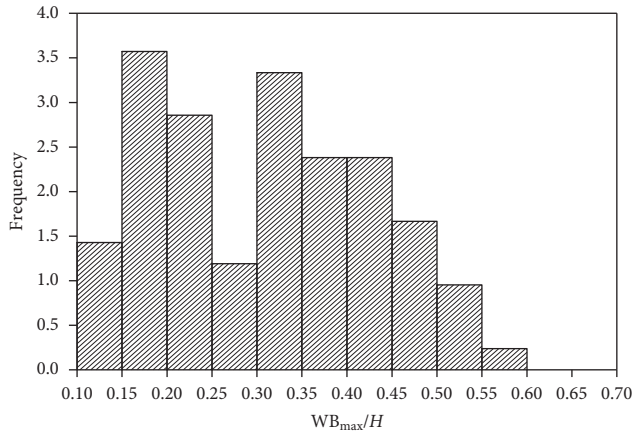

Figure 12: Frequency histogram of the maximum influence width coefficient along the Z axis.

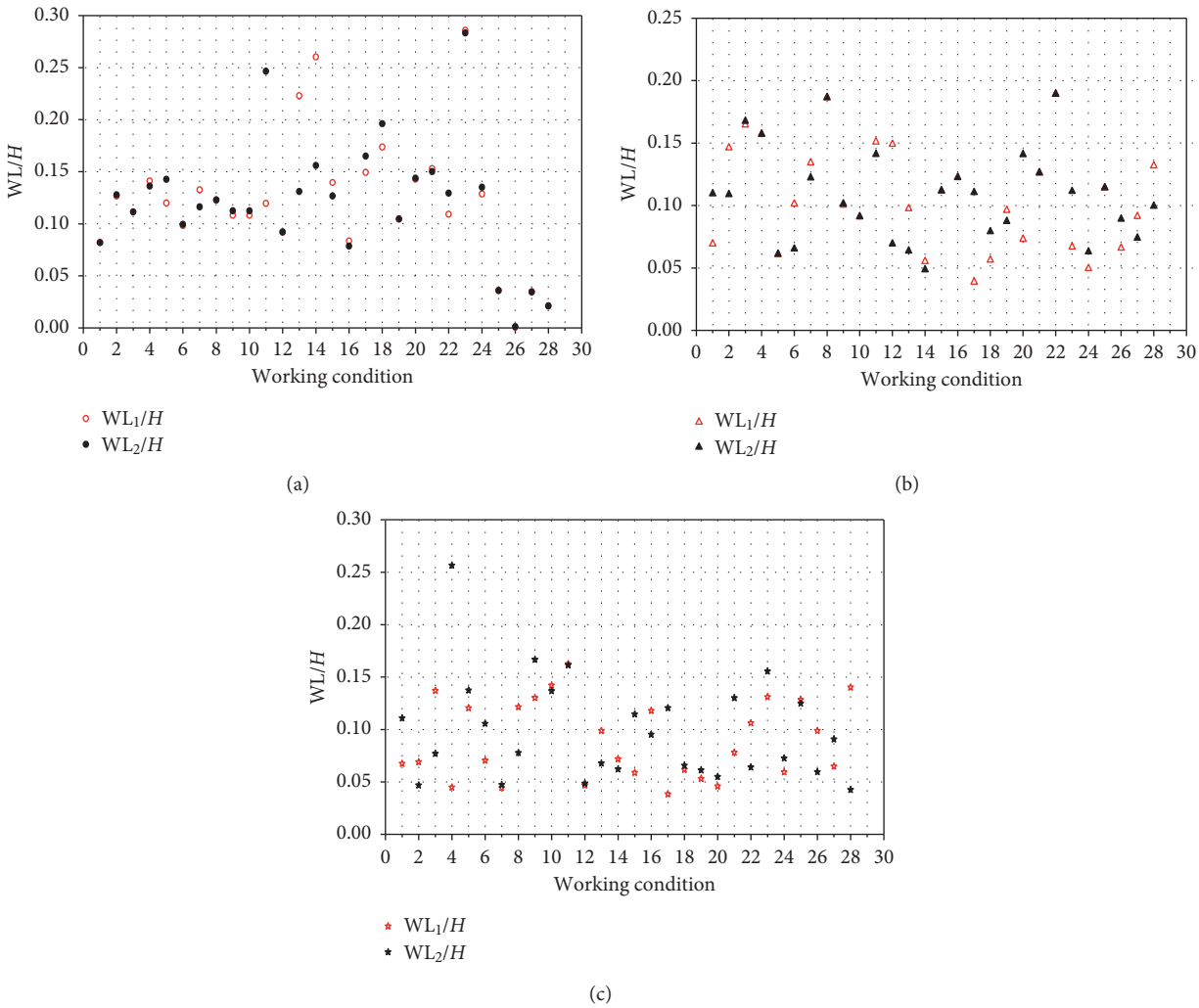

Figure 13: Width coefficient of influence along the X axis of continuous collapse of masonry structure under various working conditions. (a) The three-story masonry structure along the X axis, (b) the five-story masonry structure along the X axis, and (c) the seven-story masonry structure along the X axis.

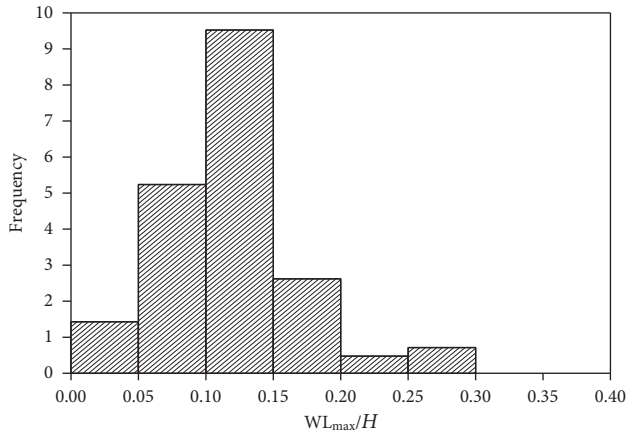

Figure 14: Frequency histogram of the maximum influence width coefficient along the X axis.

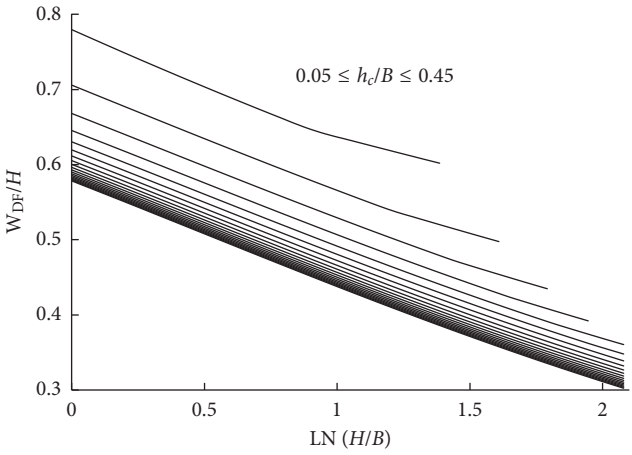

Figure 15: Coefficient change schematic diagram of structure directional collapse influence width.

collision process with the ground, and the actual movement of "flying stones" can be recorded more realistically. The second case is the "flying stones" collide with the ground in the movement process, and they fail when the deformation reaches a failure condition. In this case, the recorded movement cannot truly reflect the movement law of "flying stones." Thus, the following cases are to study the two kinds of movement law of the "flying stones."

The element numbers 12508 and 12522 of the five-story masonry structure become "flying stones" under the sixth working condition. The initial space position of elements is shown in Figure 16. Figure 17 shows the time-displacement curve of the elements in the three directions of X, Y, and Z.

According to the time-displacement curve of the flying stone elements, the flying stone elements fly at a certain initial velocity at $t = 3.32$ s, perform parabolic motion under the gravity, and have collision and friction with the ground. The velocity then gradually decreases. Element number 12508 collides with the ground at $t = 5.82$ s to reach the failure condition and loses the constraint, and then accelerates with the forces of gravity. Element number 12522 stays static on the ground after $t = 8.66$ s. In the whole process, element number 12522 conforms to the general

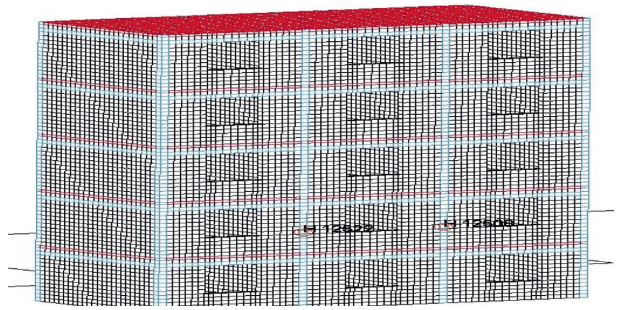

Figure 16: Initial space position of the flying stone element.

movement law, and element number 12508 does not conform to the general movement law.

Movement law of the "flying stone" element which does not fail in the collision process is more consistent with the actual situation. Table 4 shows their initial and final center-of-mass coordinates. Table 5 shows the comparison between the influence distance of the effective flying stone element and the main influence distance of the debris accumulation.

Table 5 shows that the influence distance caused by the movement of the flying stone is mostly larger than the main influence distance of the collapsed building. Thus, the influence of the flying stone generated by the structure in the collapse process should be considered fully when determining the safe distance.

5. Probability Model of Main Influence Distance

Hypothesis testing is made on the population distribution to determine the maximum main influence width coefficient distribution model of the collapsed building under earthquakes. Six kinds of probability distribution models (normal distribution, lognormal distribution, gamma distribution, extreme value type I, Rayleigh distribution, and extreme value type III) are selected, and the comparison diagrams of the frequency histogram and the empirical distribution function are used.

5.1. Assumed Distribution and Hypothesis Testing. The frequency histograms of the maximum influence width coefficient along the Z axis and X axis are compared with the assumed six probability distribution density diagrams (see Figures 18 and 19). The comparison diagrams of the corresponding empirical distribution function and theoretical six probability distribution function are shown in Figures 20 and 21. Among them, the corresponding parameters of the assumed probability distribution are shown in Table 4.

Whether the theoretical distribution of random variables represents the population distribution of the variables requires a hypothesis testing. Thus, the above assumed distributions are tested using the K-S test [38] and the chi-square test [39].

The chi-square and K-S tests of 0.05 confidence are calculated on the six assumed population distributions along the Z axis and the X axis, respectively. The results of the p value [40] are shown in Table 6.

If the significance level A is greater than the p value, then the null hypothesis is rejected at the significance level α. If A is less than the P-value, then the null hypothesis is accepted

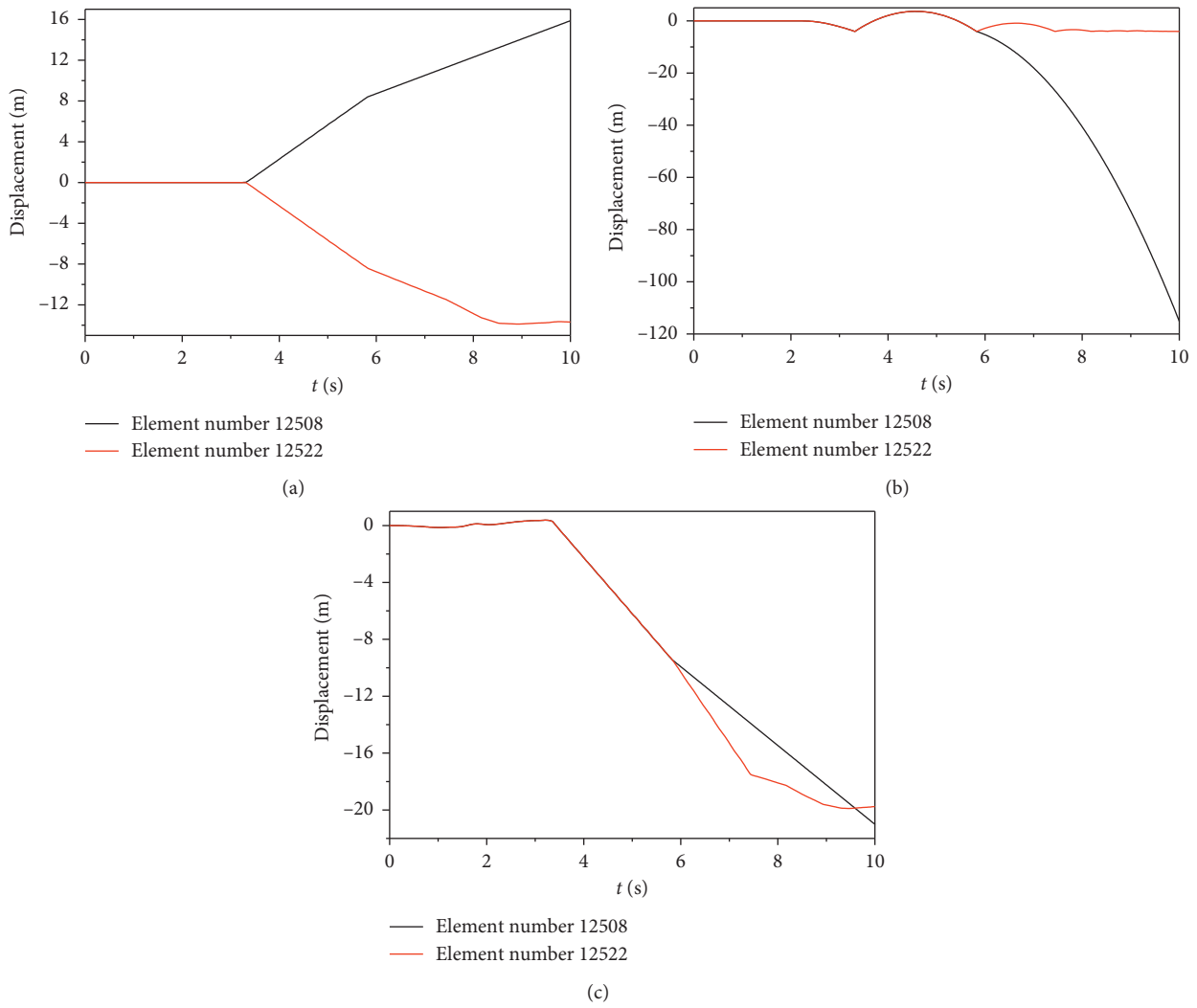

Figure 17: Time-displacement curve of the flying stone elements. (a) The direction along the X axis, (b) the direction along the Y axis, and (c) the direction along the Z axis.

Table 4: The initial and final center-of-mass coordinates of the effective flying stones element.

Model working condition	Element	Initial center-of-mass coordinate (m)			Final center-of-mass coordinate (m)		
		X_0	Y_0	Z_0	X_t	Y_t	Z_t
11, the three-story structure	9601	0.00	2.30	6.00	−6.28	0.04	22.29
	10336	13.50	2.30	6.00	19.37	0.00	22.21
16, the three-story structure	14593	4.50	4.75	0.00	6.16	0.05	−11.83
	14594	4.50	4.58	0.00	6.25	0.05	−11.71
24, the three-story structure	8728	11.92	1.86	6.00	11.69	0.03	4.41
	10336	13.50	2.30	6.00	16.39	0.01	11.22
	10324	9.00	2.30	6.00	9.44	0.00	4.60
18, the five-story structure	9601	0.00	2.30	6.00	−0.94	0.01	2.15
	18194	4.50	11.18	0.00	10.42	0.04	−11.12
26, the five-story structure	12499	4.50	4.96	6.00	11.86	0.06	15.07
27, the five-story structure	15594	4.50	6.50	6.00	−8.47	0.41	9.29
28, the five-story structure	9593	0.00	2.20	6.00	−9.70	0.08	4.41
	10038	13.50	2.20	6.00	23.20	0.08	4.43
17, the seven-story structure	15250	13.50	20.59	1.06	26.20	0.05	−5.72
	15254	13.50	20.59	1.77	26.55	0.04	−11.44

Table 5: The influence distance of effective flying stones element and the main influence distance of debris accumulation.

Model working condition	Element	$\lvert X_t - X_0 \rvert$	WL_{max}	Displacement: Z	$\lvert Z_t - Z_0 - Z \rvert$	WB_{max}
11, the three-story structure	9601	6.28	2.22	−0.68	16.97	4.94
	10336	5.87		−0.68	16.89	
16, the three-story structure	14593	1.66	0.75	0.13	11.96	3.04
	14594	1.75		0.13	11.84	
24, the three-story structure	8728	0.24	1.22	−2.56	0.97	3.41
	10336	2.89		−2.56	7.78	
	10324	0.44		−2.56	1.16	
	9601	0.94		−2.56	1.29	
18, the five-story structure	18194	5.92	1.19	−0.04	11.08	1.76
26, the five-story structure	12499	7.36	1.34	−0.01	9.08	2.64
27, the five-story structure	15594	12.97	1.37	0.03	3.26	3.60
28, the five-story structure	9593	9.70	1.98	−0.02	1.57	4.39
	10038	9.70		−0.02	1.55	
17, the seven-story structure	15250	12.70	2.53	−0.41	6.37	10.24
	15254	13.05		−0.41	12.79	

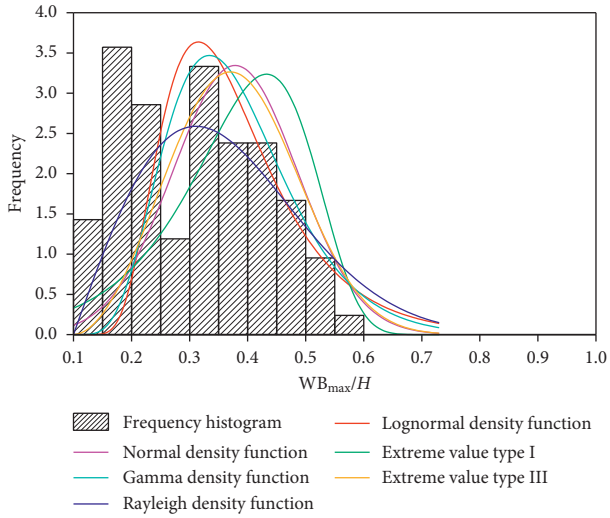

Figure 18: Frequency histogram along the Z axis and assumed distribution density functions.

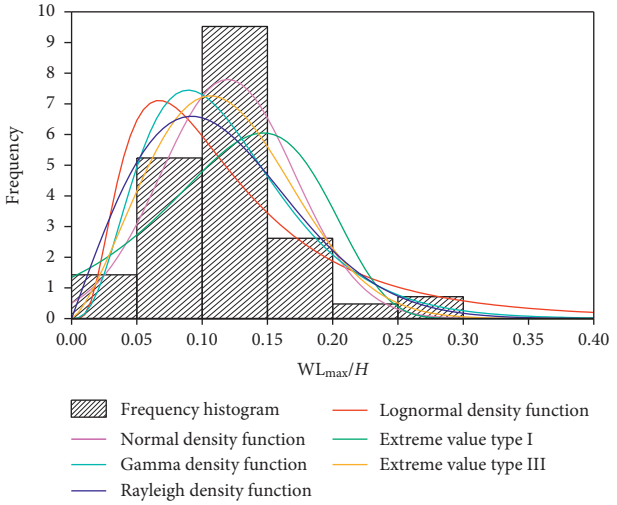

Figure 19: Frequency histogram along the X axis and assumed distribution density functions.

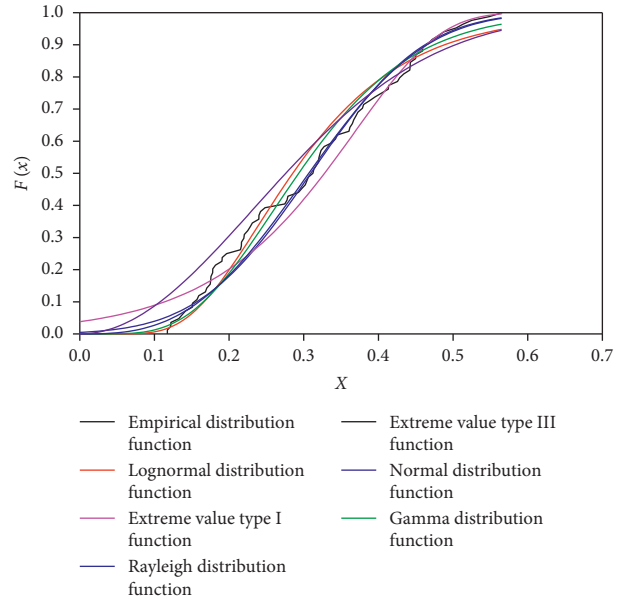

Figure 20: Empirical distribution function along the Z axis and theoretical distribution functions.

at the significance level α. Therefore, it is found in Table 4 that among the assumed distributions along the Z axis, the gamma distribution and extreme value type III are more coincident. In addition, the assumptions of normal distribution, lognormal distribution, and Rayleigh distribution are accepted, whereas the assumption of extreme type I distribution is rejected. The assumed distributions along the X axis only accept the assumption of the normal distribution and the assumptions of the other five distributions are rejected.

5.2. The Probability Model of Main Influence Distance. The number of all working conditions is N ($N = 84$). According to each calculation result, the maximum main influence width coefficient WB_{max}/H is analyzed statistically, and the number of $WB_{max}/H \geq WB_0/H$ is then counted. The probability formula of the maximum main influence of

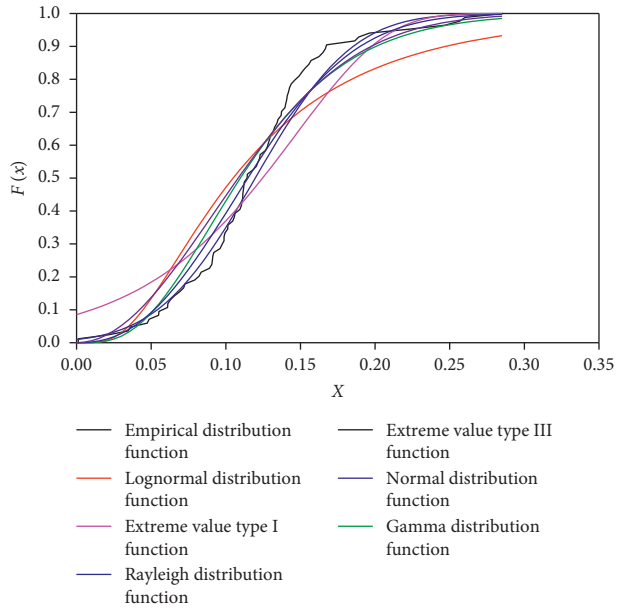

Figure 21: Empirical distribution function along the X axis and theoretical distribution functions.

Table 6: Assumed distribution parameters and p value in hypothetical testing.

Number	Assumed distribution	Parameter estimation							
		The direction along the Z axis		K-S test	Chi-square test	The direction along the X axis		K-S test	Chi-square test
1	Normal distribution	$\mu = 0.310$	$\sigma = 0.119$	0.411	0.095	$\mu = 0.120$	$\sigma = 0.003$	0.300	0.057
2	Lognormal distribution	$\mu = -1.255$	$\sigma = 0.420$	0.329	0.080	$\mu = -2.255$	$\sigma = 0.669$	0.004	0.000
3	Extreme value type I	$\mu = 0.369$	$\sigma = 0.114$	0.311	0.019	$\mu = 0.137$	$\sigma = 0.061$	0.012	0.000
4	Gamma distribution	$\alpha = 6.285$	$\beta = 0.049$	0.609	0.086	$\alpha = 3.943$	$\beta = 0.030$	0.084	0.006
5	Extreme value type III	$\lambda = 0.348$	$\kappa = 2.886$	0.541	0.130	$\lambda = 0.134$	$\kappa = 2.380$	0.330	0.028
6	Rayleigh distribution	—	$\sigma = 0.234$	0.179	0.093	—	$\sigma = 0.092$	0.024	0.002

debris accumulation after the masonry structure collapsed under earthquake excitation is

$$P\left(\frac{\mathrm{WB}_{\max}}{H} \geq \frac{\mathrm{WB}_0}{H}\right) = \frac{N_0}{N}. \quad (1)$$

The results of the maximum influence probability are shown in Figures 22 and 23.

Using the hypothesis testing of different probability distribution models, the fitting results are shown in Figures 24 and 25. It is found that along the Z axis, the gamma distribution and the extreme value type III are relatively in good agreement with the statistical results. Along the X axis, the normal distribution and the statistical result are deviated relatively, but they are consistent with each other.

6. Simplified Calculation Table of Main Influence Distance

Figures 26 and 27 show the maximum influence width coefficient along the Z axis and the X axis in the continued collapse mode of the masonry structure under the action of 84 working conditions.

It is found in Figure 26 that according to the calculation results of 84 sets, the maximum influence width coefficient along the Z axis has an envelope value of 0.5657, which may include the maximum values of all the main influence width coefficient. The envelope value of no less than 90% of the maximum influence width coefficient is 0.4672, and the envelope value of no less than 80% of the maximum influence width coefficient is 0.4341. Meanwhile, it is found in Figure 27 that the maximum value of the main influence width coefficient along the X axis has an envelope value of 0.2859. The envelope value of no less than 90% of the maximum influence width coefficient is 0.1675; and the envelope value of no less than 80% of the maximum influence width coefficient is 0.1491.

Based on Tian's research [37], combined with the statistical analysis of the above simulations, the simplified calculation table of the influence distance after the building collapsed can be obtained (see Table 7).

Based on contents of Table 7, the main influence distance of the collapsed building can be calculated. Regardless of the impact of "flying stones," the main influence distance for building collapse is the minimum distance for people and buildings after the earthquake, and the control distance of

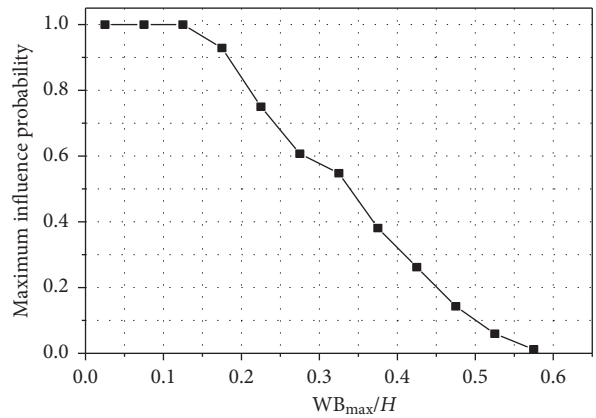

Figure 22: The maximum influence probability of the debris accumulation distribution along the Z axis under the continuous collapse of the masonry structure.

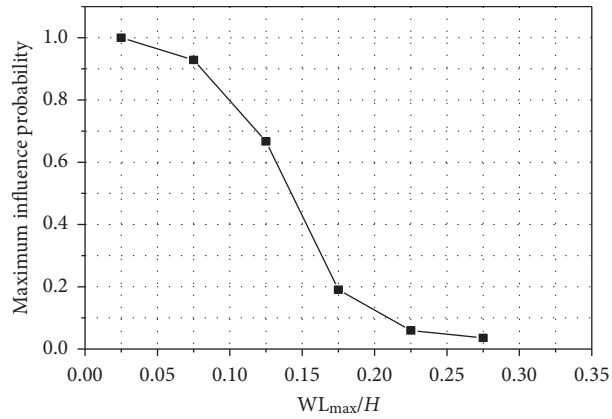

Figure 23: The maximum influence probability of the debris accumulation distribution along the X axis under the continuous collapse of the masonry structure.

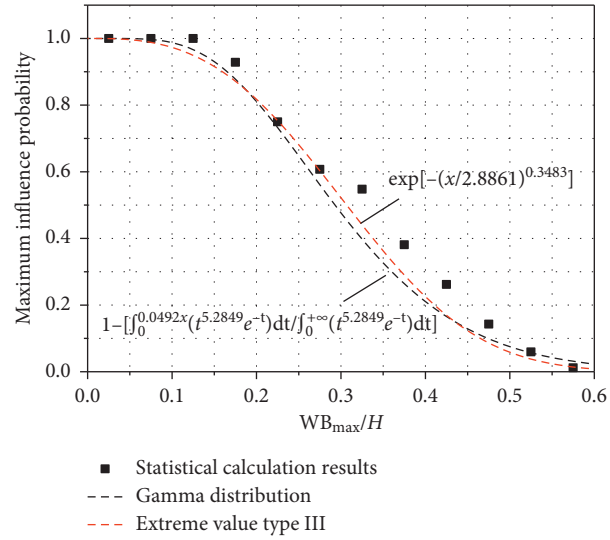

Figure 24: Fitting results of the maximum influence probability of the debris accumulation distribution along the Z axis under the continuous collapse.

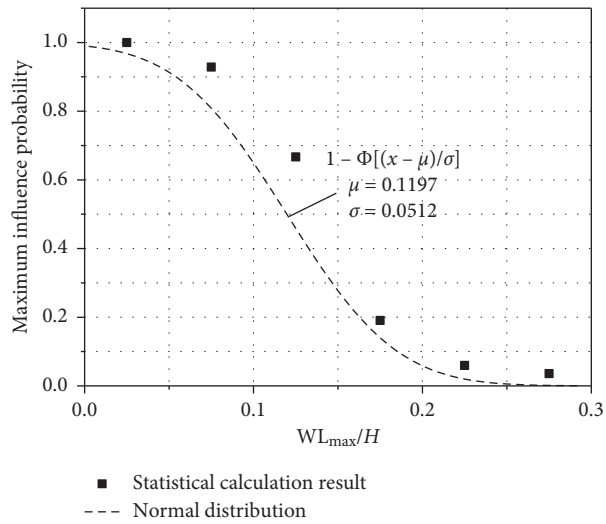

Figure 25: Fitting results of the maximum influence probability of the debris accumulation distribution along the X axis under the continuous collapse.

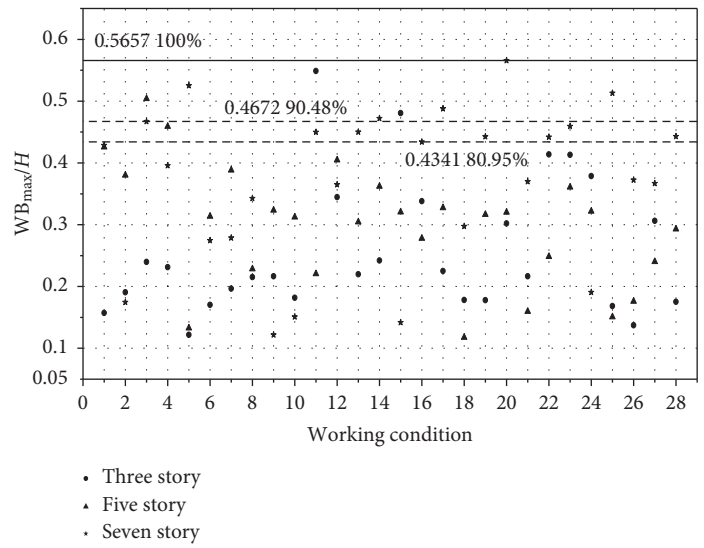

Figure 26: Statistic of the maximum influence width coefficient of the masonry structure along the Z axis under the continuous collapse mode of various working conditions.

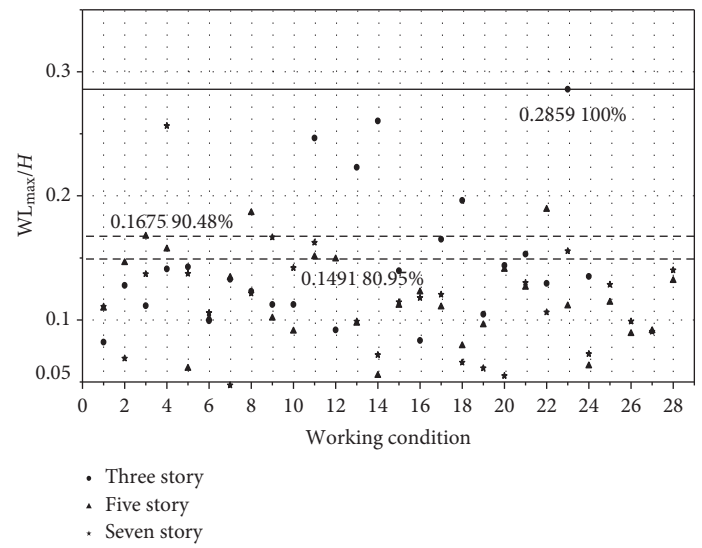

Figure 27: Statistic of the maximum influence width coefficient of the masonry structure along the X axis under the continuous collapse mode of various working conditions.

Table 7: Building collapse impact distance simplified calculation table.

Building destruction types	Disposal mode	Building height					Influence width coefficient
		<24 m	24m–54m (including 24 m)	54m–100m (including 54m)	100m–160m (including 100m)	160m–250 m (including 160m)	≥250m
Possible collapsed buildings	The long side of the building is in parallel with the red line	2/3	2/3~1/2	0.5	0.5~0.4	0.4~0.3	The coefficient should be specially studied and not less than 75m
	The long side of the building is perpendicular to the red line	0.5	0.5~0.3	0.3~0.25	0.25~0.2	0.2~0.15	The coefficient should be specially studied and not less than 38m
Uncollapsed buildings	The coefficient is determined according to the safety distance of preventing falling objects						
Remarks	The influence distance of the building collapse is calculated by the product of the height of the building exceeding the ground evaluated and the width coefficient. When the height is in the interval specified in the table, interpolation calculation can be used.						

road red lines should be planned based on the main influence distance for building collapse.

7. Conclusion

(1) The collapse modes of the masonry structure under various working conditions can be divided into three kinds: sloughing collapse, and collapse in the positive and negative directions along the Z axis. The three-story masonry structure is more prone to sloughing collapse under various seismic conditions, and the five-story and seven-story masonry structures are more likely to collapse in the positive and negative directions along the Z axis.

(2) The influence distance caused by movement of the flying stone is mostly larger than the main influence distance of the collapsed building. Thus, the influence of the flying stone generated by the structure in the collapse process should be considered fully when determining the safe distance.

(3) Among the assumed distributions along the Z axis, the gamma distribution and extreme value type III are more coincident. In addition, the assumptions of normal distribution, lognormal distribution, and Rayleigh distribution are accepted, whereas the assumption of extreme type I distribution is rejected. The assumed distributions along the X axis only accept the assumption of the normal distribution, and the assumptions of the other five distributions are rejected.

(4) Through the simulation of the five-story masonry structure, the maximum influence width coefficient along the Z axis has an envelope value of 0.5657. Meanwhile, the maximum value of the main influence width coefficient along the X axis has an envelope value of 0.2859.

(5) Combined with the previous research of the research group, a simplified calculation table of the impact distance after a building collapse is obtained, which provides the basis for the minimum distance that people should be away from the building after the earthquake and the road red line planning of urban road traffic.

Data Availability

The data used to support the findings of this study are available from the corresponding author upon request.

Conflicts of Interest

The author(s) declare no potential conflicts of interest with respect to the research, authorship, and/or publication of this article.

Acknowledgments

This study was supported by the National Natural Science Foundation of China (Grant no. 51678017), National Key R&D Program of China (Grant nos. 2018YFD1100902-1), and Research Project on Major Policy Theory and Practice of China Earthquake Administration (CEAZY2019JZ14).

References

[1] Y. D. Liang, J. Z. Jiang, Y. Li et al., "Study on concrete structure earthquake damage prediction method," *Journal of North China Institute of Science and Technology*, vol. 12, no. 1, pp. 112–117, 2015.

[2] Z. P. Song, M. G. Zhang, and J. Liu, *Disaster Information Catalog of Global Earthquakes*, Seismological Press, Beijing, China, 2011.

[3] Y. M. Li and L. P. Liu, *Disaster Investigation and Study Report of Sichuan Wenchuan Earthquake*, Chongqing University Press, Chongqing, China, 2008, in Chinese.

[4] Department of Homeland Security Federal Emergency Management Agency, *Hazus Mr4 Earthquake Tech Manual*, Federal Emergency Management Agency, Washington, DC, USA, 2003.

[5] K. Meguro and M. Hakuno, "Simulation of collapse of structures due to earthquakes using the extended distinct element method," in *Proceedings of the 10th World Conference on Earthquake Engineering, WCEE 1992*, pp. 3793–3796, Madrid, Spain, July 1992.

[6] J. X. Song and J. Li, "Simulation of urban transportation system connectivity after the earthquake," *Journal of Natural Disasters*, vol. 5, no. 1, p. 73, 1996.

[7] H. X. Guo, "Debris distribution prediction and graphic display of building damages and collapse," Master thesis, Tsinghua University, Beijing, China, 1993.

[8] S. Argyroudis, *Contribution to seismic vulnerability and risk of transportation networks in urban environment*, Ph.D. thesis, Aristotle University of Thessaloniki, Thessaloniki, Greece, 2010.

[9] S. Argyroudis, J. Selva, P. Gehl, and K. Pitilakis, "Systemic seismic risk assessment of road networks considering interactions with the built environment," *Computer-Aided Civil and Infrastructure Engineering*, vol. 30, no. 7, pp. 524–540, 2015.

[10] Y. Z. Zhao, Y. C. Chen, and J. Y. Zheng, "Discrete element simulation of the breakage and collapse of masonry structures," *Chinese Journal of Computational Mechanics*, vol. 28, no. 4, pp. 523–529, 2011.

[11] C. X. Fu, "Study on typical seismic collapse pattern of RC frame structure," Master thesis, Institute of Engineering Mechanics, China Earthquake Administration, Beijing, China, 2014.

[12] S. W. Yang, *Experimental study on collapse mechanism of multi-story RC frame school buildings*, Ph.D. thesis, Institute of Engineering Mechanics, China Earthquake Administration, Beijing, China, 2015.

[13] F. L. Zhao, "Simulation analysis for collapse of reinforced concrete frame structures under earthquake based on the discrete element method," Master thesis, Tongji University, Shanghai, China, 2008.

[14] X. L. Gu, Q. H. Huang, and X. L. Wang, "Spatial collapse responses of reinforced concrete frame structures under earthquakes-test study and numerical simulation," *China Civil Engineering Journal*, vol. 45, no. 9, pp. 36–45, 2012.

[15] Q. Tan, Y. M. Li, Y. Tang et al., "Collapse process prediction and reasonableness analysis of masonry structures subjected to strong earthquake," *Journal of PLA University of Science and Technology (Natural Science Edition)*, vol. 14, no. 4, pp. 415–420, 2013.

[16] Y. Hu, "Study on failure mode and collapse mechanism of masonry structures under earthquakes," Master thesis, Institute of Engineering Mechanics, China Earthquake Administration, Beijing, China, 2014.

[17] D. Y. Tang, X. Z. Lu, and P. L. Ye, "Influence of axial compression ratio to the seismic collapse resistance of RC frame structures," *Earthquake Resistant Engineering and Retrofitting*, vol. 42, no. 5, pp. 26–35, 2010.

[18] P. Negro and G. Verzeletti, "Effect of infills on the global behaviour of R/C frames: energy considerations from pseudodynamic tests," *Earthquake Engineering & Structural Dynamics*, vol. 25, no. 8, pp. 753–773, 1996.

[19] A. Furtado, H. Rodrigues, H. Varum, and A. Costa, "Evaluation of different strengthening techniques efficiency for a soft-storey building," *European Journal of Environment and Civil Engineering*, vol. 21, no. 4, pp. 371–388, 2016.

[20] Q. H. Huang, *Study on spatial collapse responses of reinforced concrete frame structures under earthquake*, Ph.D. thesis, Tongji University, Shanghai, China, 2006.

[21] Q. H. Huang, S. N. Huang, X. Z. Lu et al., "A primary study on the secondary disasters induced by the damage of high-rise building envelops under earthquake," *Engineering Mechanics*, vol. 30, pp. 94–98, 2013.

[22] Z. B. Xie, X. Z. Lu, Z. Xu et al., "Experimental research and range of injury risk analysis of earthquake-induced hazard of falling exterior infill walls," *Journal of Natural Disasters*, vol. 27, no. 1, pp. 17–26, 2018.

[23] D. H. Ma, O. Y. Tian, and W. Wang, "Study on vertical progressive-collapse of frame structure by earthquake," *Journal of Shenyang Jianzhu University (Natural Science)*, vol. 30, no. 4, pp. 667–675, 2014.

[24] G. X. Zhao, H. Chen, and J. Li, "Urban transportation system Assessment and reconstruction after the earthquake," *World Earthquake Engineering*, vol. 3, pp. 6–10, 1996.

[25] R. W. Clough and J. Penzien, *Dynamics of Structures*, McGraw-Hill, New York, NY, USA, 1993.

[26] D. D. Kong, Y. H. Zhao, P. Wang et al., "Equivalent moduli of reinforced concrete in simulating analysis," *Journal of Shenyang Architectural and Civil Engineering Institute*, vol. 19, no. 3, pp. 165–168, 2003.

[27] C. X. Shi, *Masonry Structure Theory and Design*, China Architecture & Building Press, Beijing, China, 2003.

[28] G. Q. Liu, *The research on the basic mechanical behavior of masonry structure*, Ph.D. thesis, Hunan University, Changsha, China, 2005.

[29] Ministry of Housing and Urban-Rural Development of the People's Republic of China (MOHURD), *Code for Design of Concrete Structures (GB50010-2010)*, China Architecture &Building Press, Beijing, China, 2010, in Chinese.

[30] LS-DYNA, *Keywords User's Manual Volume II (Version 971)*, Livermore Software Technology Corporation, Livermore, CA, USA, 2007.

[31] ANSYS, *ANSYS Release 10.0 Documentation for ANSYS*, ANSYS, Inc., Houston, TX, USA, 2004.

[32] Ministry of Housing and Urban-rural Development of the People's Republic of China (MOHURD), *Code for Design of Masonry Structure (GB50003-2011)*, China Architecture &Building Press, Beijing, China, 2011, in Chinese.

[33] Y. X. Hu, *Earthquake Engineering*, Seismological Press, Beijing, China, 1998.

[34] L. M. Zhang and X. L. Liu, "Forward research of collapse analysis of reinforced concrete structures," *Earthquake Engineering and Engineering Vibration*, vol. 23, no. 3, pp. 47–52, 2003.

[35] J. Yu, Y.-P. Gan, J. Wu, and H. Wu, "Effect of concrete masonry infill walls on progressive collapse performance of reinforced concrete infilled frames," *Engineering Structures*, vol. 191, pp. 179–193, 2019.

[36] S. Li, M. M. Kose, S. Shan, and H. Sezen, "Modeling methods for collapse analysis of reinforced concrete frames with infill walls," *Journal of Structural Engineering*, vol. 145, no. 4, Article ID 04019011, 2019.

[37] Q. Y. Tian, "A study on influence scope assessment of seismic collapse building," Master thesis, Beijing University of Technology, Beijing, China, 2014.

[38] B. W. Cheng, Y. L. Wang, L. F. Shi et al., "Lognormal distribution law of science and technology scale indicators," *Science of Science and Management of S.& T,* vol. 21, no. 9, pp. 9–11, 2000.

[39] D. Y. Fu and J. Wang, "Exploration on the statistical test system of correspondence analysis," *Statistics & Information Forum*, vol. 25, no. 3, pp. 3–6, 2010.

[40] D. M. Fan, "*P* value in the hypothesis testing," *Journal of Zhengzhou Economic Management Institute*, vol. 14, no. 2, pp. 70-71, 2002.